Spatiotemporal characterisation of Fire Severity Over a 23 Year Period in South-East Queensland using data collected with Landsat sensors: A preliminary study

B.M. Parker [a*], T. Lewis [b], S.K. Srivastava [a]

[a] *School of Science and Engineering, Faculty of Science Health Education and Engineering, University of the Sunshine Coast, Maroochydore DC, Qld 4558, Australia*

[b] *Department of Agriculture, Fisheries and Forestry, Agri-Science Queensland University of the Sunshine Coast, Locked Bag 4, Maroochydore DC, Qld 4558, Australia*

Land management agencies are increasingly using multispectral satellite imagery to monitor post-fire ground conditions to guide effective conservation and asset protection management strategies. Estimates derived from such data can span over multiple decades and can be analysed to identify spatiotemporal burnt area patterns. Interestingly, fire severity is rarely derived from multi-decadal remote sensing datasets. Accordingly, in this study we explored the utility of imagery captured with Landsat sensors (5 TM, 7 ETM+ and 8 OLI) to characterise fire severity of burnt areas over a 23 year period in a national park with a woodland and heath ecosystem. The multi-temporal differenced normalised burn ratio (dNBR) was used to estimate fire severity for individual burnt areas, which were then aggregated to identify spatiotemporal patterns. Accuracy assessment was achieved using ground truth data collected with the Geometrically Structured Composite Burn Index (GeoCBI), which incorporates the fraction of cover (FCOV) of vegetation over the total plot. Our results indicated that Landsat imagery was ideal for significantly estimating fire severity (accuracy = 72 %, kappa = 0.63, $P = < 0.001$) in sclerophyll woodland and heath ecosystems. Further, we had interesting insight into the patterns of increased fire severity within specific vegetation types and across the study site.

Keywords: multi-decadal fire severity patterns; Landsat; GeoCBI; dNBR; heath; woodland.

1. Introduction

Fire plays an important role in the ecosystem dynamics of Australian fire-prone vegetation communities (Parr and Andersen 2006; Tran and Wild 2000). The fire regime is central to vegetation-fire dynamics and is comprised of the variables: season, frequency, spatial and temporal extent, and intensity (Gill 1975). However, European settlement has substantially altered the fire regimes that Australian fire-prone ecosystems are adapted too (Enright and Thomas 2008; Gill 2008). These changes vary across Australia and have included total fire suppression in some areas, and increased fire frequency in others (Penman *et al.* 2011). Both can lead to poor ecosystem health and the former to increased fuel load accumulation and connectivity, which under optimal climatic factors can result in large intense wildfires (Miller and Urban 2000; Penman *et al.* 2011). Returning fire regimes to a pre European state will prove difficult, and in many fragmented landscapes may not be

possible (Gill 2008). Thereafter, the goal is to implement fire regimes that protect human assets, and enhance, or at least conserve biodiversity (Penman *et al.* 2011).

The economic feasibility combined with extended spatial and temporal coverage of remotely sensed data are ideal for empirically analysing spatial patterns of burnt areas and associated ecological responses at the community level (Benson and MacKenzie 1995; Kelly *et al.* 2012; Kerr and Ostrovsky 2003; Lentile *et al*. 2006). This is most pronounced in inaccessible locations where field surveys are either impractical or require huge resources. Furthermore, archives of the Landsat 5 TM, 7 ETM+ and 8 OLI sensors (now referred to as Landsat) contain datasets at 30m spatial resolution, and temporal resolution as frequently as 8 days dating back to 1984. These archives can be used to reliably infer long-term fire associated ecosystem patterns (Driscoll *et al. 2010)*. Multispectral remote sensing methods have been used to estimate the frequency, season and heterogeneity of burnt areas over multiple decades (Duncan *et al.* 2009; Durieut and Ryan 1997; Srivastava *et al.* 2013). Multi-decadal estimates of fire severity have received little attention, although, Hammill & Bradstock (2006) have identified it as a future research priority. Fire severity is a measure of the biomass consumed by the fire as derived from remote sensing methods while fire intensity is a measure of energy output from the active fire (Keeley 2009). Within similar vegetation types, fire severity measurements can be used as a surrogate for fire intensity, this is due to the generally high relationship and that post-fire fire severity can easily be quantified using remote sensing methods (Murphy and Russell-Smith 2010). Landsat images, in conjunction with the multi-temporal band ratio index dNBR, have been widely used to classify burnt area and fire severity in vegetated landscapes (reviewed in French *et al.* 2008; Key and Benson 2006; Srivastava *et al.* 2013).

Multispectral remote sensing of burnt areas is not without its drawbacks. The utility of remotely sensed data is limited for detecting sub-canopy low severity burnt areas under dense green canopy cover (Arroyo *et al.* 2008; De Santis and Chuvieco 2009; Kolden *et al.* 2012). The GeoCBI field validation fire severity index attempts to correct for this by integrating FCOV measurements as a weighting factor into the total plot fire severity measurement. Thereby, as FCOV increases, a proxy for canopy cover, the total plot fire severity rating decreases. This produces field measurements that are more closely related to Landsat dNBR fire severity classifications (De Santis and Chuvieco 2009). Thus GeoCBI more consistently relates to a wider range of fire severities as derived from Landsat dNBR classifications (De Santis and Chuvieco 2009). Although the GeoCBI-dNBR provides an improved relationship over other field validation methods, low severity surface burnt areas under tall dense canopy are still difficult to detect (De Santis and Chuvieco 2009).

This paper describes the methods used in a preliminary study to: 1) estimate the spatial and temporal extent and frequency of low, moderate and high fire severity classes; 2) evaluate the relationship between Landsat dNBR classifications and GeoCBI field validation data.

2. Material and methods

Study area

Research was conducted in the Mooloolah River National Park/conservation area (MRNP), in South East Queensland (Figure 1). MRNP consists of a north and south section dissected by a dual-lane motorway (Figure 1).
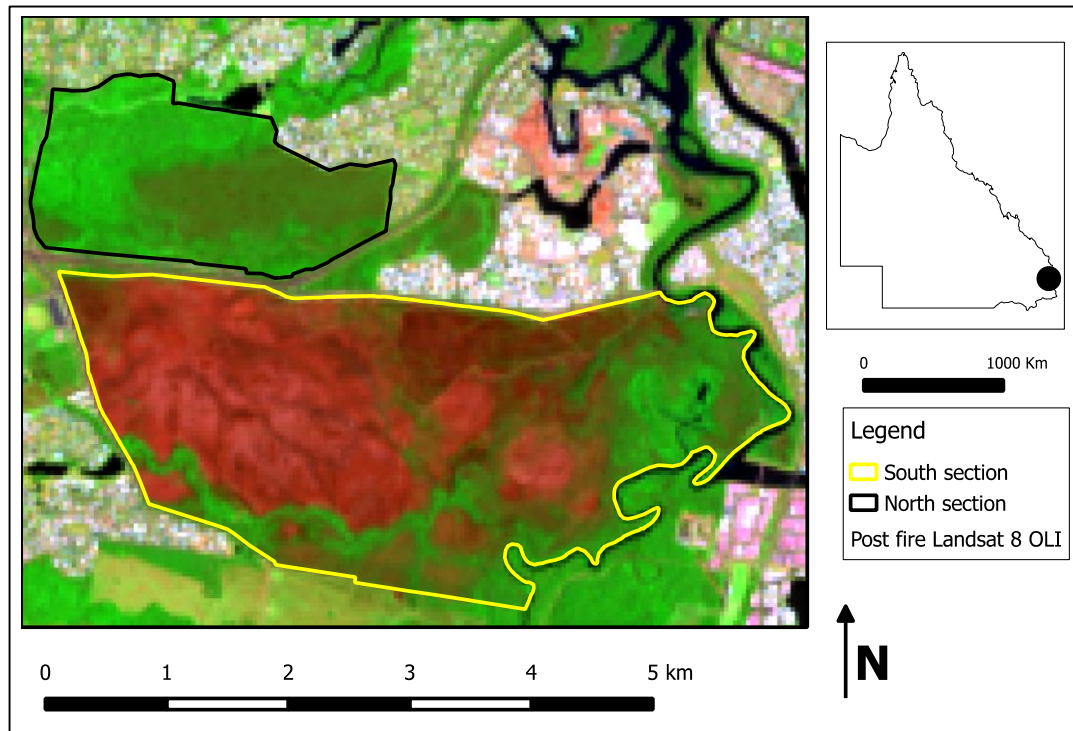
Figure 1. The 2013 burnt area in the south section of MRNP is visually identifiable as maroon in colour, as captured by the Landsat 8 OLI sensor. The false colour composite image was created with SWIR 2, NIR, and red spectral bands.

The vegetation of MRNP consisted of sclerophyll woodland and heath communities, detailed summaries of vegetation classes are compiled by Accad *et al.* (2008). In brief, heath communities were characterised as structurally dense single-story wet and dry vegetation classes growing to less than two meters tall. Woodlands were characteristic of an open structure mostly less than 20 meters tall with a heath and graminoid understory, and an occasional shrubby midstorey three to eight meters high. Fragments of tall closed Eucalyptus forest occurred in the northwest of the north section and estuarine communities fringed a river on the east side of the south section.

GeoCBI field measurements

Field measurements were taken six months after the December 2013 fire. Although vegetation regeneration processes had begun, signs of fire severity were still apparent. The total plot FCOV was visually estimated using a spherical densitometer. Measurements were taken four times at four evenly spaced points recorded 7.5 meters from the plot centre and averaged. To avoid issues with miss-registration sampling plots were at least 60 meters apart and were centred in the middle of at least 2x2 pixel aggregates with a variation in dNBR values of less than five precent. This reduces the introduction of field and imagery geo-rectification error, and autocorrelation of reflectance from surrounding pixels (Congalton 1991; Key and Benson 2006). Clusters of 3x3 homogeneous pixel are recommended for field sampling sites (Congalton 1991; Key and Benson 2006), however they only occurred in the high severity classes. Pixel centre coordinates of sample point locations were uploaded onto a Trimble Geoexplorer 6000 series differential GPS and used for field navigation. Once at the field sample point the plot centre coordinates were recorded and later corrected using gnss correction logs collected by Geoscience Australia (2014) at their Caboolture station (approximately 50 Km South of MRNP). After

differential corrections were applied, the estimated accuracy of field sample point were 45% >15cm, 98% >2m and 100% >5m.

Burnt area data

The Department of National Parks, Recreation, Sports and Racing (DNPRSR) hold fire perimeter maps and fire reports for most national parks in Queensland, which for MRNP dated back to 1970. Perimeter maps were used to locate Landsat images acquired for path 89 and row 79 as standard level one terrain corrected (L1T) products from the United States Geological Survey (USGS) Earth Explorer (2014) archive. Landsat images were obtained as close to the pre and post ignition dates as possible. Exact dates of three fire events are unknown due to incomplete fire reports. However, the maximum known interval between a fire event and image capture was 68 days (Table 1). This was attributed to interference from cloud cover and shadow that precluded burnt area classification. Ignition dates and Landsat image characteristics used for fire severity classifications are provided (Table 1).

Table 1. Landsat images and fire dates used to estimate MRNP fire severity over the 23 year study period.

Ignition date		Landsat capture date	Days after fire	Sun elevation (°)
December 1991	Pre	8th October 1991		48.80
	Post	27th December 1991		53.45
2nd November 1992	Pre	24th September 1992		44.04
	Post	27th November 1992	25	55.01
26th January 1993	Pre	27th November 1992		55.01
	Post	4th April 1993	68	37.92
21st November 1994	Pre	30th September 1994		44.97
	Post	20th January 1995	60	47.64
1996	Pre	3rd September 1996		36.86
	Post	6th November 1996		54.03
1998	Pre	8th August 1998		33.07
	Post	11th October 1998		52.69
23rd July 2000	Pre	2nd June 2000		31.03
	Post	21st August 2000	29	38.68
29th August 2000	Pre	21st August 2000		38.68
	Post	22nd September 2000	31	49.12
9th September 2000	Pre	21st August 2000		38.68
	Post	22nd September 2000	13	49.12
13th August 2002	Pre	10th July 2002		29.71
	Post	27th August 2002	14	39.88
1st January 2007	Pre	18th November 2006		62.31
	Post	6th February 2007	36	54.52
2nd September 2009	Pre	2nd August 2009		38.68
	Post	23rd September 2009	21	49.28
10th October 2009	Pre	23rd September 2009		49.28
	Post	11th October 2009	33	60.93
7th December 2013	Pre	4th October 2013		55.18
	Post	23rd December 2013	16	62.09

The spectral resolution of data acquired from Landsat sensors has been described (Figure 2). Spatial resolutions for Landsat multispectral bands are 30m, and the panchromatic band captured by 7 ETM+ and 8 OLI sensors is 15m.

Table 2. Spectral band resolutions acquired by Landsat 8 OLI, 7 ETM+ and 5 TM sensors.

Spectral band	Wavelength (μm)			Bandwidth (μm)		
	OLI	**ETM+**	**TM**	**OLI**	**ETM+**	**TM**
Costal Blue	0.433-0.453			0.020		
Blue	0.450-0.515	0.452-0.514	0.452-0.518	0.065	0.062	0.66
Green	0.525-0.600	0.519-0.601	0.528-0.609	0.080	0.082	0.081
Red	0.630-0.680	0.631-0.692	0.626-0.693	0.050	0.061	0.067
Near Infrared	0.845-0.885	0.772-0.898	0.776-0.904	0.040	0.126	0.128
Short Wave Infrared 1	1.560-1.660	1.547-1.748	1.567-1.784	0.100	0.201	0.217
Short Wave Infrared 2	2.100-2.300	2.065-2.346	2.097-2.349	0.200	0.281	0.252
Panchromatic	0.500-0.680	0.515-0.896		0.165	0.381	

Image rectifications

Georectification

All the images used in this study were geo-rectified with a high resolution four band aerial image (near infrared, red, green and blue), captured in 2008 with a horizontal accuracy of $\pm$ 0.30 meters, obtained from the Sunshine Coast Regional Council. Landsat images were geo-rectified using a first order polynomial transformation with root mean square error (RMSE) of less than five meters. This study applied recommendations by Hughes *et al.* (2006) to use hard features for the geo-rectification of satellite and aerial images. Hard features, that generally include man-made structures such as the corners of buildings and road intersections, are discrete and contain distinct corners that remain stationary over time, thus provide increased accuracy as ground control points in multi-temporal image analysis. The coordinate system applied to all datasets used in this study was WGS 84 UTM zone 56S.

Radiometric conversion

Radiometric conversions were performed to allow for direct comparison between images acquired on different dates, at different view angles and between Landsat satellite sensors. Radiometric conversion to spectral radiance at-sensor's aperture was achieved (Equation 1) (Chander et al., 2009). This was followed by conversion to top of atmosphere (TOA) (Equation 2) (Chander et al., 2009).

$$Lsat_\lambda \ = \ G_\lambda * DN_\lambda + O_\lambda \qquad (1)$$

where $Lsat_\lambda$ is the satellite radiance in W m^{-2} sr^{-1} μm^{-1} for band λ, G_λ and O_λ are the gain and offset respectively, for band λ specific spectral at-sensor radiances in W m^{-2} sr^{-1} μm^{-1}, and DN_λ is the raw band λ specific pixel.

$$TOA_\lambda \ = \ \frac{(Lsat_\lambda * d^2 * \pi)}{(ESUN_\lambda * Cos(90 - \theta))} \qquad (2)$$

where TOA_λ is unitless, d is the earth sun distance, $ESUN_\lambda$ is the band λ specific exoatmospheric irradiance in W m^{-2} sr^{-1} μm^{-1} and θ is the solar elevation angle. $ESUN_\lambda$ values for 5 TM and 7 ETM+ sensors are reported (Chander *et al.* 2009), and 8 OLI (Vanhellemont and Ruddick 2014). The metadata text file provided with

Landsat files contain the date of image capture and solar elevation for the entire scene, gain (RADIANCE_MULTI_BAND) and offset (RADIANCE_ADD_BAND) for each band. Earth sun distance was determined by converting the date of image capture to day-of-year then using the look up table provided by Chander *et al.* (2009).

Image normalisation

Radiometric consistency between multi-temporal datasets is a requirement for detecting earth surface changes such as fire severity (Vicente-Serrano *et al.* 2008), and to accurately apply fire severity detection thresholds retrospectively (Salvador *et al. 2000)*. Since this study used a Landsat dataset that spanned 23 years a stringent image normalisation method was vital. Radiometric normalisation methods can be absolute, where pixel values are converted to their true surface values, or relative, where pixel values are calibrated to values of a common reference image. Absolute radiometric calibration models such as 6S radiative transfer codes require the sensors spectral profile and atmospheric property codes, the latter of which generally is not available for retrospective studies (Du *et al.* 2002). While absolute radiometric calibration models such as dark object subtraction contains simplified assumptions that can significantly introduce error into the analysis (Furby and Campbell 2001; Vicente-Serrano *et al.* 2008). Relative radiometric normalisation methods are widely used due to their simplicity and accuracy for producing multi-temporal datasets with comparable values (Chen *et al.* 2005; Furby and Campbell 2001). Relative atmospheric correction can be achieved be fitting pseudo invariant features (PIF) to a linear regression model. PIF are targets on Earth's surface that can be assumed to remain stable in reflectance over long time periods and thereby changes in their pixel values can be associated with radiometric noise (Chen *et al.* 2004; Furby and Campbell 2001; Vicente-Serrano *et al.* 2008). PIF targets should include house and building rooftops, roads, quarries and deep water (Vicente-Serrano *et al.* 2008). Through linear regression model fitting, atmospheric contamination can be reduced by selecting the reference image as cloud free and with the least haze (Furby & Campbell 2001). Cloud is generally associated with increased atmospheric water vapour (Furby and Campbell 2001).

Relative atmospheric correction was achieved by fitting values from 154 PIF points to a linear regression model. The reflectance values captured by PIF were well spread across the spectral range of Landsat bands. PIF targets were manually selected, and the same pixel locations were sampled over all images. This method reduced the possibility of statistical outliers caused by dramatic land-use change that can occur with automated PIF selection methods. Linear regression of PIF values was used to derive gain and offset coefficients to be used for image normalisation (Equation 3). This relationship assumes that linear atmospheric effects outweigh non-linear effects (Furby and Campbell 2001; Vicente-Serrano *et al.* 2008).

$$DN_{NORM\lambda} = G_\lambda * DN_{SUB\lambda} + O_\lambda \qquad (3)$$

where DN_{NORM} are normalised band λ pixel values, G and O are the gain and offset derived from PIF linear regression values and DN_{SUB} are band λ pixel values to be normalised.

Accuracy of image normalisation can be assessed with measures of RMSE. The RMSE is a measure of response variable variation (normalised images) from the model prediction (reference image used for atmospheric normalisation). Smaller

RMSE implies a reduction in noise between the reference and normalised image, thus improving the multi-temporal consistency of image datasets (McGovern *et al.* 2002). The RMSE between TOA un-normalised and normalised bands was measured to gauge the effectiveness of PIF linear regression to produce temporally homogeneous images. RMSE was conducted with a set of 57 independent PIF targets. All normalised images produced RMSE values of less than one precent, the threshold set by McGovern *et al.* (2002) to assess image normalisation success.

Fire severity detection and classification

The NBR index measures change in the spectral response caused by fire, especially to vegetation (Equation 4) (Figure 2 D) (Key 2006). The pre-fire NBR can be subtracted from the post-fire NBR classifications as in the multi-temporal spectral index dNBR (Equation 5) (Figure 2 E) to detect absolute change in spectral reflectance between the pre and post fire images.

$$NBR \ = \ \frac{(SWIR - NIR)}{(SWIR + NIR)} \tag{4}$$

$$dNBR = \ preNBR - postNBR \tag{5}$$

where the Landsat spectral bands $SWIR$ and NIR are short wave infrared and near infrared respectively.

Increasingly positive dNBR values correspond with a greater change between the pre and post NBR classifications. Burnt area pixel values in the NIR band decrease, and are associated with reduced photosynthetically active vegetation (Figure 2 B) (Key 2006). While in the SWIR band increases in pixel values are associated with reduced photosynthetically active vegetation, moisture content, ash deposition and increased soil exposure (Figure 2 C) (Key 2006).
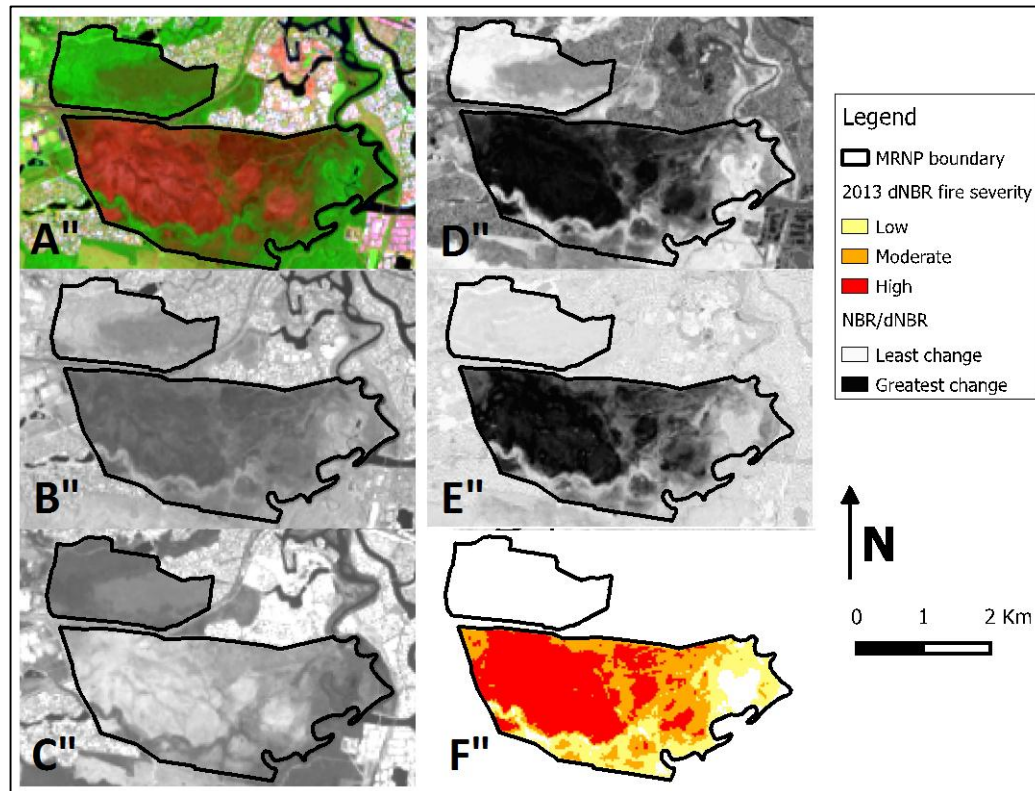
Figure 2. The dNBR classification process as applied to the 2013 burnt area. (A) The post fire Landsat 8 OLI false colour composite image is created with SWIR 2, NIR, and red spectral bands. (B) The NIR band is used in NBR to detect spectral changes associated with reduced photosynthetically active vegetation. (C) The SWIR band is used in NBR to detect spectral changes associated with photosynthetically active vegetation, moisture content, ash deposition and increased soil exposure. (D) The NBR discrete post-fire classification. (E) The dNBR discrete fire severity classification. (F) The discrete fire severity classification.

The continuous dNBR data classifications were reclassified into four discrete severity classes: unburnt; low; moderate and high fire severity (Figure 2 F). The GeoCBI contains discrete values that can be used to classify field data into fire severity classes, that in turn can be used to guide dNBR discrete fire severity classifications (Miller and Thode 2007) with the combination of mid-point threshold values (Hammill and Bradstock 2006). The lower and upper threshold values used for discrete fire severity classification of GeoCBI field data are presented (Table 3) (Miller and Thode 2007).

Table 3. Upper and lower fire severity thresholds used for discrete classification of GeoCBI field data.

Fire severity class	Lower threshold	Upper threshold
Unburnt	0.00	0.09
Low	0.10	1.24
Moderate	1.25	2.24
High	2.25	3.00

dNBR discrete classification was achieved by extracting the pixel values that corresponded with GeoCBI field sample points. These pixel values were grouped into fire severity classes based on their GeoCBI rating, and a mean dNBR pixel value was derived for each class. Midpoint values were then derived between each of the

adjoining dNBR class means. Finally the mid-point values were used as thresholds for discrete dNBR fire severity reclassification.

Multi-decadal fire severity analysis

The fire severity thresholds created for the 2013 classification were extrapolated to the dNBR classifications of retrospective burnt areas in this study. The discrete fire severity classifications for each fire event were then aggregated to produce pixel based estimates of the frequency for low, moderate and high fire severity classes. Time-since-fire estimates were also produced that incorporated fire severity into each vegetation age class.

Accuracy assessment

A confusion matrix accuracy assessment was used to validate remotely sensed dNBR classifications against GeoCBI field data (Congalton 1991). The Kappa statistic was used as a measure of agreement to determine whether the classification was better than that produced by chance alone (Congalton 1991). Landis and Koch (1977) developed a scale (Table 4) to provide consistency when determining the strength of the Kappa statistic measurement for categorical data as used in this study.

Table 4. The discrete scale used to determine the strength of the Kappa statistic.

Kappa statistic	Strength of agreement
0.0 - 0.2	Slight
0.2 - 0.4	Fair
0.4 - 0.6	Moderate
0.6 - 0.8	Substantial
0.8 - 1.0	Almost perfect

Although this scale is arbitrary it provides a standard to assess the Kappa statistic measure (Landis and Koch 1977).

Software and data analysis

Image and statistical analysis were preformed on R statistics software 3.0.3 (R Core Team 2014) with the packages: raster; Landsat (Goslee 2011); caret and maptools.

QGIS 2.2.0 was used for image visualisation and cartographical map production (QGIS Development Team 2014).

3. Results

Accuracy of Landsat fire severity estimations

The linear regression model fitted to continuous GeoCBI-dNBR values for the 2013 fire was significantly high ($r^2 = 0.8072$, $P = < 0.001$) (Figure 3). This indicated a strong linear relationship between the GeoCBI field data collection method and Landsat derived dNBR fire severity classification.
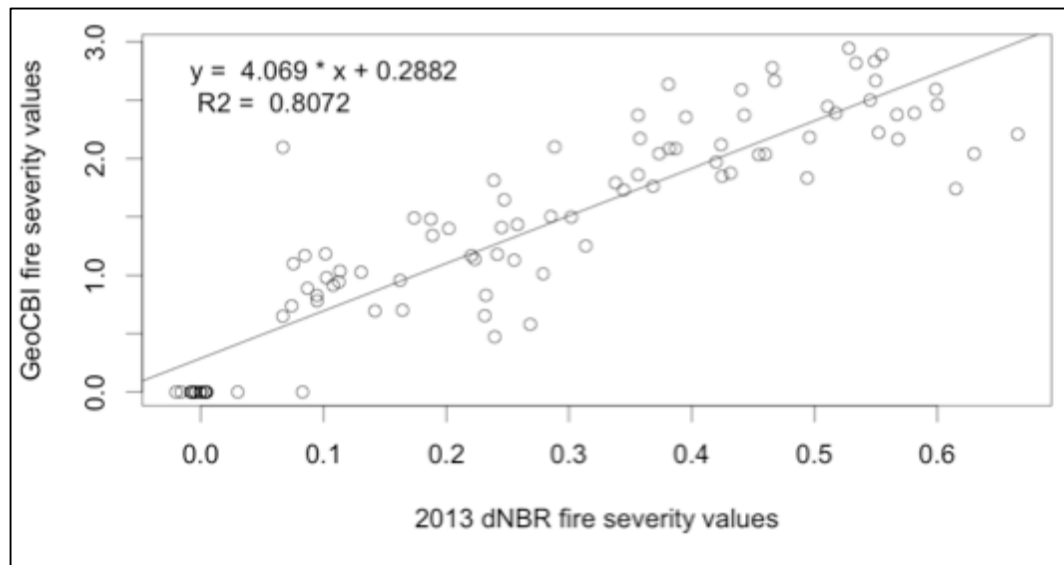
Figure 3. Fire severity measurements for the a burnt area in a heath and woodland ecosystem. The linear relationship between GeoCBI field values and dNBR values derived from Landsat data for the 2013 burnt area are shown.

The 2013 Landsat dNBR classification provided an estimate of discrete fire severity classes with an accuracy of 72 % that represented substantial agreement (kappa = 0.63, $P = < 0.001$) with discrete GeoCBI classes (Table 5), as classified using GeoCBI threshold values (*Fire severity detection and classification* section).

Table 5. Confusion matrix for 2013 Landsat 8 OLI derived dNBR fire severity classification, between extracted cell value count for each fire severity class and corresponding GeoCBI fire severity count.

		Field data				Total	User's accuracy	
	Severity*	0	1	2	3	Total	User's accuracy	
2013 dNBR	0	18	1	1	0	20	90 %	
	1	1	21	7	0	29	72 %	
	2	0	3	17	5	25	68 %	
	3	0	0	9	14	23	61 %	
	Total	19	25	34	19		**Kappa**	0.63
Producer's accuracy		95 %	84 %	50 %	74 %		***P* value**	< 0.001
							Accuracy	72 %

*Severity classes are: 0-unburnt, 1-low severity, 2-moderate severity, 3-high severity, and grey boxes represent the number of correct classifications in each class. 97 samples collected. (α 0.05)

The fire severity thresholds generally produced classes with high agreement between dNBR classifications and GeoCBI field data. Unburnt, low and high dNBR fire severity classes provided substantial to near prefect measures of agreement. While moderate fire severity estimations yielded the lowest agreement with field data (producer's accuracy 50 %), indicating under-estimation of moderate fire severity classes. Further, confusion between moderate and high classes (n = 14) is evident in the confusion matrix (Table 5).

Frequency of fire severity in MRNP

Mapped fire severity estimations for the frequency of high, moderate and low fire severity classes were identified. The occurrence of high fire severity was mostly confined to heath vegetation communities (figure 4).
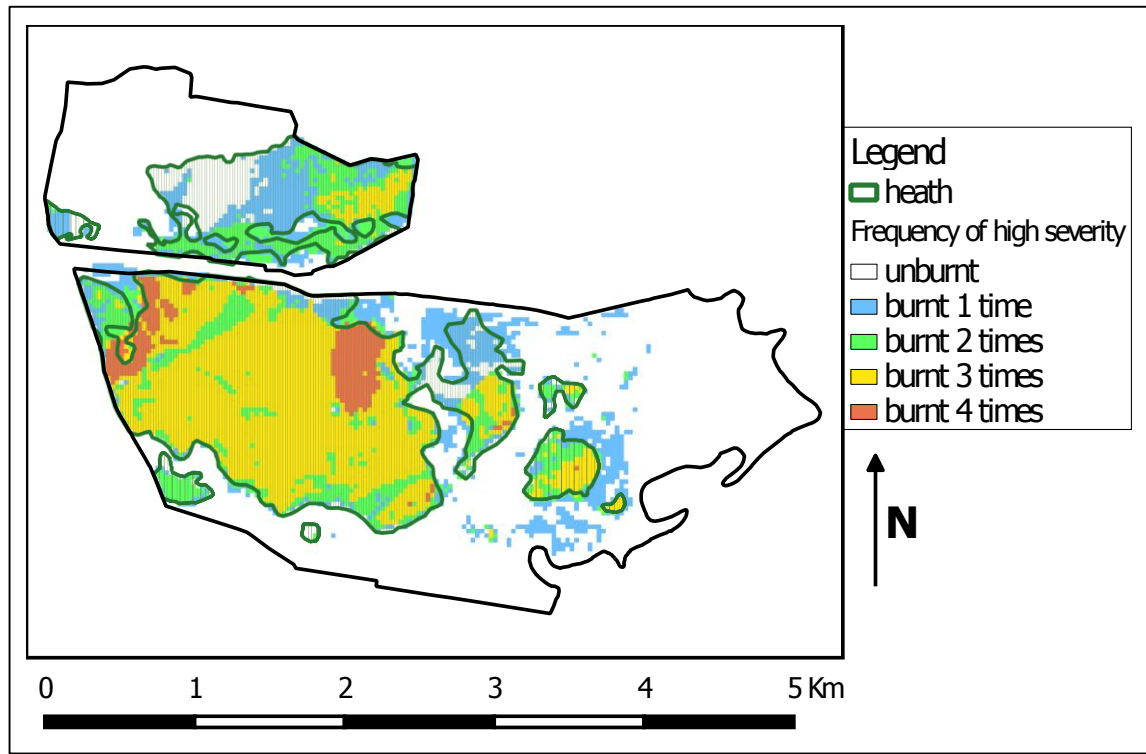

Figure 4. Frequency of high fire severity in MRNP over a 23 year period.

In this preliminary study patterns of moderate fire severity were not visible (Figure 5).
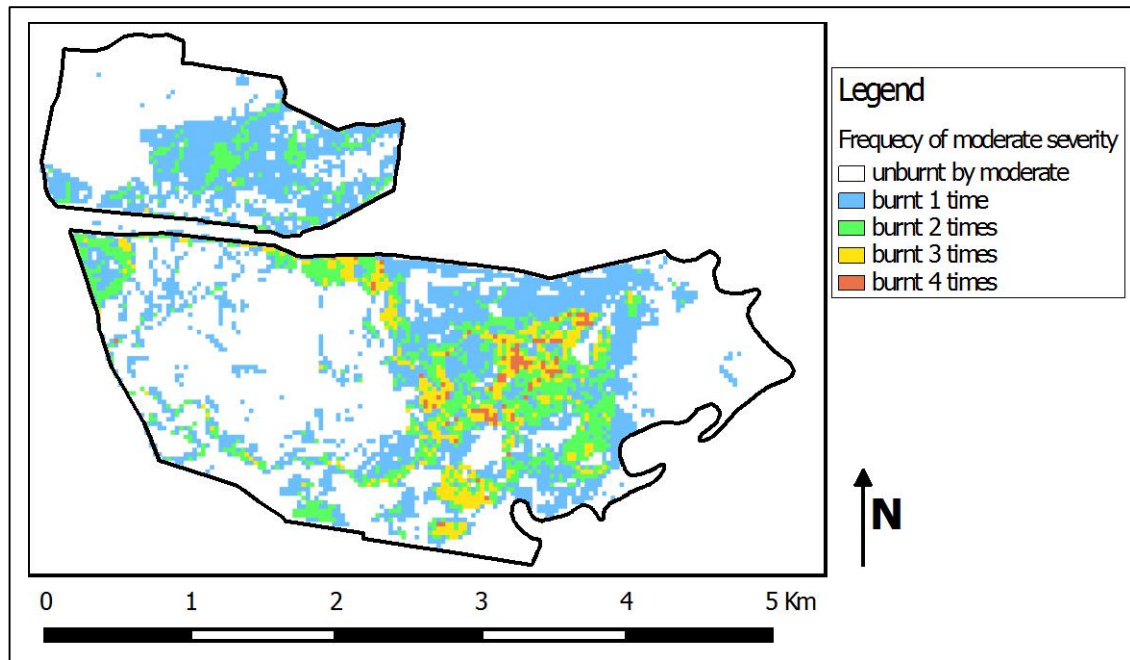

Figure 5. Frequency of moderate fire severity in MRNP over a 23 year period.

Low fire severity was more widespread than moderate and high fire severity, and there was an increased occurrence within Melaleuca woodlands in the south section of MRNP (Figure 6).
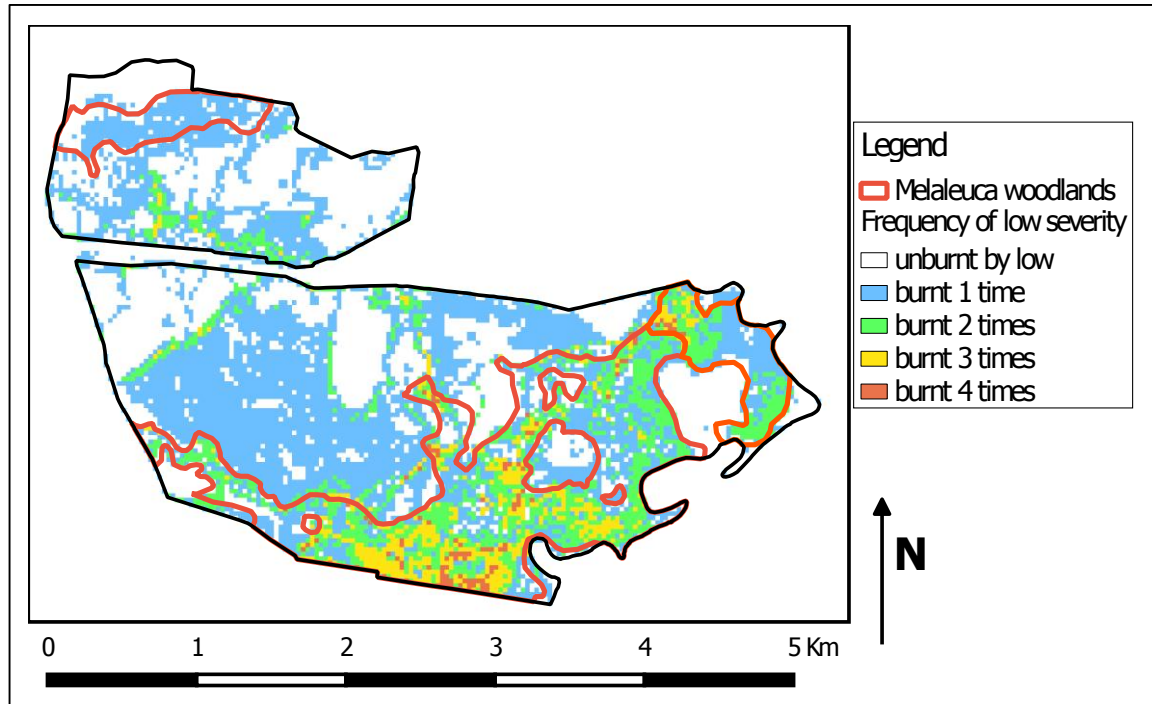

Figure 6. Frequency of low fire severity in MRNP over a 23 year study period.

High frequency (three and four times burnt), high severity burnt areas were most common in heath vegetation communities. In all fire severity classes, increased frequency occurred in the south section of MRNP compared to the north section.

Time-since-fire estimates with the inclusion of fire severity classes in each vegetation-age-class have been mapped (Figure 7).
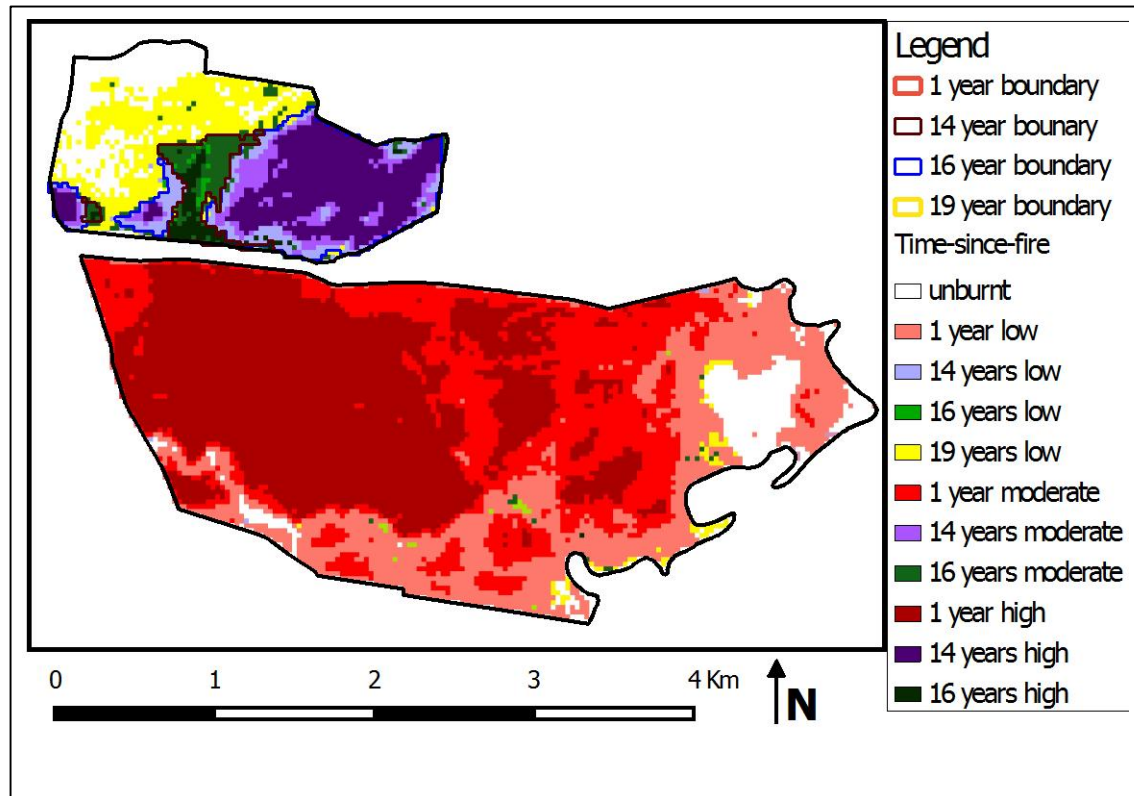
Figure 7. Fire severity classes within each time-since-fire age class.

The spatial homogenisation of the 2013 burnt area is evident by the nearly exclusive one year time-since-fire age class in the south section of MRNP (Figure 7). In comparison the north section consisted of three vegetation age classes that span over a five year period (Figure 7). The south section of MRNP was dominated by a one year time-since-fire vegetation age class. Whereas the north section was characterised by a heterogeneous time-since-fire mosaic containing long unburnt 14 - 19 year vegetation age classes. Throughout MRNP, sections of long unburnt (> 23 years) vegetation existed (Figure 7). In the south section these long unburnt patches were comprised mainly of estuarine communities, and in the north section by tall closed Eucalyptus forests. It should be noted that estuarine communities did not exist in the north section, nor did tall closed Eucalyptus forests in the south section.

4. Discussion

We found that Landsat data in combination with GeoCBI field surveys can provide accurate estimates of multi-decadal fire severity patterns. This was attributed to the significantly high linear relationship and confusion matrix accuracies achieved between the 2013 dNBR classifications and GeoCBI field data. Further, PIF linear regression model fitting reduced the RMSE between normalised and TOA images to a level acceptable to validate the extrapolation of the 2013 fire severity class thresholds over retrospective dNBR classifications. The linear relationship between Landsat and field data indicated that the GeoCBI-dNBR relationship provided a consistent measure of fire severity across the range of locations sampled in MRNP. The majority of confusion matrix error was attributed to the under-estimation of moderate fire severity class as classified using the Landsat dNBR index. This finding was consistent with Miller *et al.* (2009), who attributed the reduced accuracy of moderate severity classes to mixed spectral responses of low and high fire severity effects. During field

surveys we found that many moderate severity sample locations contained highly heterogeneous mixes of moderate and low-end high severity variables. This was particularly apparent in vegetation where some GeoCBI variables were rated as high severity due to total foliage consumption, while other variables were rated as low severity as resprouting was vigorous and vegetation mortality was low. The GeoCBI was designed for North American and Mediterranean European fire-prone ecosystems that are dominated by obligate seeder species whose general response to at least 100 % foliage scorch is death (Crandall and Platt 2012; Santana *et al.* 2012) unlike many Australian fire-prone species that vigorously resprout from lignotuber and epicormic buds, even after high severity fire (Burrows 2013). We suggest that minor changes to the GeoCBI may be required to better suit Australian fire-prone ecosystems. This aside, the combinations of remote sensing techniques and field surveys used in this study for multi-decadal estimates of fire severity can provide new insight into ecological appropriateness and fire behaviour.

The Landsat archive provided us with the unique opportunity to characterise fire severity in a sclerophyll woodland and heath ecosystem over a 23 year period. Multi-decadal burnt area estimates derived from Landsat and associated ancillary datasets are significantly recognised to provide the detailed information required for ecologically appropriate fire regime implementation (Srivastava *et al.* 2013), and can be improved with fire severity data. In this preliminary study we identified several patterns of fire severity in MRNP. Heath vegetation communities were most frequently burnt and constituted for the majority of high severity burnt areas. This co-insides with findings that Australian heath is highly flammable and generally the majority of biomass is consumed by fires (Griffith *et al.* 2003). Hammill & Bradstock (2006) attributed the high biomass consumption of heath due to their short height and highly connected vertical fuel structure. Melaleuca vegetation communities, on the other hand, constituted for the majority of the frequently burnt low severity areas. The incorporation of fire severity estimates into time-since-fire vegetation age classes further identified heterogeneous spatial patterns that occurred due to the MRNP fire regime. We identified that the south section of MRNP received increased frequency of all fire severity classes and contained an even time-since-fire vegetation age class. The north section contained older time-since-fire vegetation age classes with the youngest being 14 years old. This is not ideal, as time-since-fire increases vegetation quickly grows to its pre-fire fuel load and can become highly connected, both vertically and horizontally, encouraging large intense fires (Miller and Urban 2000). Although, small patches should remain long unburnt to provide habitat for species that require deep litter (Clarke 2008).

Based on DNPRSR fire perimeter maps, we successfully estimated the spatial extent of all burnt areas that occurred in MRNP over the 23 year period (unpublished data). The fire perimeter maps and fire reports supplied by DNPRSR provided a full fire history and allowed us to acquire Landsat data as close, pre and post fire, to the ignition dates as possible. Although unavoidable where fire history is unknown, studies that obtained a set number of images (2-4) per year at set times periods (3-6 months apart) (Duncan *et al.* 2009), can miss burnt areas due to rapid regrowth, as occurs in heath, sedge and grassland communities (Hammill and Bradstock 2006; Mcfarland 1988; Miller and Thode 2007; Russell-Smith *et al.* 2012). Although we did sample low severity burnt areas under a maximum canopy FCOV of 70 - 83 % (n = 3), due to small sample size this is an area that requires further research.

Conclusion

We demonstrated the utility of Landsat derived dNBR fire severity classifications in combination with GeoCBI field validation to accurately characterise multi-decadal spatial patterns of fire severity in native heath and woodland ecosystems. The GeoCBI field validation was successfully used to produce discrete dNBR fire severity classes, which, with prudent image normalisation methods were extrapolated over retrospective burnt areas. This study has identified the significantly enhanced fire regime information that can be derived from the Landsat data archive. Multi-decadal estimates provide potentially useful data for managers and ecologists to better understand the long-term ecological patterns and impacts of fire severity. We recognise the importance of the Landsat data archive, it was ideal for this study due to the consistent, continuous and scientifically rigorous data, which extends back to 1984. Further research is required to assess the accuracy of Landsat and other multi-decadal remote sensor archives to estimate fire severity across varying vegetation types, especially in tall closed canopies.

Acknowledgments

Reference

Accad, A., Neldner, V.J., Wilson, B. A., & Niehus, R.E. (2008) Remnant Vegetation in Queensland. Analysis of remnant vegetation 1997-1999-2000-2001-2003-2005, including regional ecosystem information. Brisbane: Queensland Herbarium, *Environmental Protection Agency*.

Arroyo, L., Pascual, C., & Manzanera, J. (2008) Fire models and methods to map fuel types: The role of remote sensing. *Forest Ecology and Management*, vol. 256, pp. 1239–1252.

Benson, B.J., & MacKenzie, M.D. (1995) Effects of sensor spatial resolution on landscape structure parameters. *Landscape Ecology*, vol. 10, pp. 113–120.

Burrows, G.E. (2013) Buds, bush fires and resprouting in the eucalypts. *Australian Journal of Botany*, vol. 61, pp. 331–349.

Chander, G., Markham, B.L., & Helder, D.L. (2009) Summary of current radiometric calibration coefficients for Landsat MSS, TM, ETM+, and EO-1 ALI sensors. *Remote Sensing of Environment*, vol. 113, pp. 893–903.

Chen, X., Vierling, L., & Deering, D. (2005) A simple and effective radiometric correction method to improve landscape change detection across sensors and across time. *Remote Sensing of Environment*, vol. 98, pp. 63–79.

Chen, X., Vierling, L., Rowell, E., & DeFelice, T. (2004) Using lidar and effective LAI data to evaluate IKONOS and Landsat 7 ETM+ vegetation cover estimates in a ponderosa pine forest. *Remote Sensing of Environment*, vol. 91, pp. 14–26.

Clarke, M.F. (2008) Catering for the needs of fauna in fire management: science or just wishful thinking?. *Wildlife Research*, vol. 35, pp. 385–394.

Congalton, R.G. (1991) A Review of Assessing the Accuracy of Classifications of Remotely Sensed Data. *Remote Sensing of Environment*, vol. 46, pp. 35–46.

Crandall, R.M., & Platt, W.J. (2012) Habitat and fire heterogeneity explain the co-occurrence of congeneric resprouter and reseeder Hypericum spp. along a Florida pine savanna ecocline. *Plant Ecology*, vol. 213, pp. 1643–1654.

De Santis, A., & Chuvieco, E. (2009) GeoCBI: A modified version of the Composite Burn Index for the initial assessment of the short-term burn severity from remotely sensed data. *Remote Sensing of Environment*, vol. 113, pp. 554–562.

Driscoll, D., Lindenmayer, D., Bennett, A., Bode, M., Bradstock, R., Cary, G., Clarke, M., Dexter, N., Fensham, R., Friend, G., Gill, M., James, S., Kay, G., Keith, D., Macgregor, C., Russell-smith, J., Salt, D., Watson, J., Williams, R., & York, A. (2010) Fire management for biodiversity conservation : Key research questions and our capacity to answer them. *Biological Conservation*, vol. 143, pp. 1928–1939.

Du, Y., Teillet, P.M., & Cihlar, J. (2002) Radiometric normalization of multitemporal high-resolution satellite images with quality control for land cover change detection. *Remote Sensing of Environment*, vol. 82, pp. 123–134.

Duncan, B.W., Shao, G., & Adrian, F.W. (2009) Delineating a managed fire regime and exploring its relationship to the natural fire regime in East Central Florida, USA: A remote sensing and GIS approach. *Forest Ecology and Management*, vol. 258, pp. 132–145.

Earth Explorer. Available online:. Available online: http://earthexplorer.usgs.gov/ (accessed on 15 March 2014).

Enright, N.J., & Thomas, I. (2008) Pre-European Fire Regimes in Australian Ecosystems. *Geography Compass*, vol. 2, pp. 979–1011.

French, N., Kasischke, E., Hall, R., Murphy, K., Verbyla, D., Hoy, E., & Allen, J. (2008) Using Landsat data to assess fire and burn severity in the North American boreal forest region: an overview and summary of results. *International Journal of Wildland Fire*, vol. 17, pp. 443–462.

Furby, S.L., & Campbell, N.A. (2001) Calibrating images from different dates to " like-value " digital counts. *Remote Sensing of Environment*, vol. 77, pp. 186–196.

Geoscience Australia. Avaliable online:. ftp://ftp.ga.gov.au/geodesy-outgoing/gnss/logs/ (accessed on 7th July 2014).

Gill A.M. (1975) Fire and the Australian flora: a review. *Australian Forestry*, vol. 38, pp. 4-25.

Gill, A.M. (2008) Underpinnings of fire management for biodiversity conservation in reserves: fire and adaptive management.

Goslee, S.C. (2011) Analyzing Remote Sensing Data in R : The landsat Package. *Journal of Statistical Software*, vol. 43, pp. 1-25.

Griffith, S.J., Bale, C., Adam, P., & Wilson, R. (2003) Wallum and related vegetation on the NSW North Coast : description and phytosociological analysis. *Cunninghamia*, vol. 8, pp. 202–252.

Hammill, K., & Bradstock, R. (2006) Remote sensing of fire severity in the Blue Mountains: influence of vegetation type and inferring fire intensity. *International Journal of Wildland Fire*, vol. 15, pp. 213.

Keeley, J. (2009) Fire intensity, fire severity and burn severity: a brief review and suggested usage. *International Journal of Wildland Fire*, vol. 18, pp. 116–126.

Kelly, L.T., Nimmo, D.G., Spence-Bailey, L.M., Taylor, R.S., Watson, S.J., Clarke, M.F., & Bennett, A.F. (2012) Managing fire mosaics for small mammal conservation: a landscape perspective. *Journal of Applied Ecology*, vol. 49, pp. 412–421.

Kerr, J.T., & Ostrovsky, M. (2003) From space to species: ecological applications for remote sensing. *Trends in Ecology & Evolution*, vol. 18, pp. 299–305.

Key, C., & Benson, N. (2006) Landscape Assessment (LA) Sampling and Analysis Methods.

Key, C.H. (2006) Ecological and Sampling Constraints on Defining Landscape Fire Severity. *Fire Ecology*, vol. 2, pp. 34–59.

Kolden, C. A., Lutz, J. A., Key, C.H., Kane, J.T., & van Wagtendonk, J.W. (2012) Mapped versus actual burned area within wildfire perimeters: Characterizing the unburned. *Forest Ecology and Management*, vol. 286, pp. 38–47.

Landis, J.R., & Koch, G.G. (1977) The Measurement of Observer Agreement for Categorical Data. *Biometrics*, vol. 33, pp. 159–174.

Lentile, L., Holden, Z., Smith, A., Falkowski, M., Hudak, A., Morgan, P., Lewis, S., Gessler, P., & Benson, N. (2006) Remote sensing techniques to assess active fire characteristics and post-fire effects. *International Journal of Wildland Fire*, vol. 15, pp. 319–345.

Mcfarland, D. (1988) Fire and the Vegetation Composition and Structure of Subtropical Heathlands in South-eastern Queensland. *Australian Journal of Botany*, vol. 36, pp. 533–546.

McGovern, E., Holden, N., Ward, S., & Collins, J. (2002) The radiometric normalization of multitemporal Thematic Mapper imagery of the midlands of Ireland - a case study. *International Journal of Remote Sensing*, vol. 23, pp. 751–766.

Miller, C., & Urban, D.L. (2000) Connectivity of forest fuels and surface fire regimes. *Landscape Ecology*, vol. 15, pp. 145–154.

Miller, J.D., Knapp, E.E., Key, C.H., Skinner, C.N., Isbell, C.J., Creasy, R.M., & Sherlock, J.W. (2009) Calibration and validation of the relative differenced Normalized Burn Ratio (RdNBR) to three measures of fire severity in the Sierra Nevada and Klamath Mountains, California, USA. *Remote Sensing of Environment*, vol. 113, pp. 645–656.

Miller, J.D., & Thode, A.E. (2007) Quantifying burn severity in a heterogeneous landscape with a relative version of the delta Normalized Burn Ratio (dNBR). *International Journal of Remote Sensing*, vol. 109, pp. 66–80.

Murphy, B.P., & Russell-Smith, J. (2010) Fire severity in a northern Australian savanna landscape: the importance of time since previous fire. *International Journal of Wildland Fire*, vol. 19, pp. 46–51.

Parr, C., & Andersen, A. (2006) Patch mosaic burning for biodiversity conservation: a critique of the pyrodiversity paradigm. *Conservation biology*, vol. 20, pp. 1610–1619.

Penman, T.D., Christie, F.J., Andersen, N.A., Bradstock, R.A., Cary, G.J., Henderson, M.K., Price, O., Tran, C., Wardle, G.M., Williams, R.J., & York, A. (2011) Prescribed burning: how can it work to conserve the things we value?. *International Journal of Wildland Fire*, vol. 20, pp. 721.

QGIS Development Team (2014) QGIS Geographic Information System. Open Source Geospatial Foundation Project. Available online: http://qgis.osgeo.org

R Core Team (2014) R: A language and environment for statistical computing. R Foundation for Statistical Computing, Vienna, Austria. Available online: http://www.R-project.org/.

Russell-smith, J., Durieut, R., & Ryan, P.G. (1997) A LANDSAT MSS-derived fire history of Kakadu National Park, monsoonal northern seasonal extent , frequency and patchiness. *Journal of Applied Ecology*, vol. 34, pp. 748–766.

Russell-Smith, J., Edwards, A.C., & Price, O.F. (2012) Simplifying the savanna: the trajectory of fire-sensitive vegetation mosaics in northern Australia. *Journal of Biogeography*, vol. 39, pp. 1303–1317.

Salvador, R., Valeriano, J., Pons, X., & Diaz-Delgado, R. (2000) A semi-automatic methodology to detect fire scars in shrubs and evergreen forests with Landsat MSS time series. *International Journal of Remote Sensing*, vol. 21, pp. 655–671.

Santana, V.M., Baeza, M.J., & Maestre, F.T. (2012) Seedling establishment along post-fire succession in Mediterranean shrublands dominated by obligate seeders. *Acta Oecologica*, vol. 39, pp. 51–60.

Srivastava, S., King, L., Mitchell, C., Wiegand, A., Carter, R., Shapcott, A., & Russell-smith, J. (2013) Ecological implications of standard fire-mapping approaches for fire management of the World Heritage. *International Journal of Wildland Fire*, vol. 22, pp. 381–393.

Tran, C., & Wild, C. (2000) A Review of Current Knowledge and Literature to Assist in Determining Ecologically Sustainable Fire Regimes for the Southeast Queensland Region. *Griffith University and the SEQ Fire and Biodiversity Consortium*.

Vanhellemont, Q., & Ruddick, K. (2014) Remote Sensing of Environment Turbid wakes associated with offshore wind turbines observed with Landsat 8. *Remote Sensing of Environment*, vol. 145, pp. 105–115.

Vicente-Serrano, S., Pérez-Cabello, F., & Lasanta, T. (2008) Remote Sensing of Environment Assessment of radiometric correction techniques in analyzing vegetation variability and change using time series of Landsat images. *Remote Sensing of Environment*, vol. 112, pp. 3916–3934.